Electronic Supplementary Material (ESI) for Physical Chemistry Chemical Physics.

[**Supporting Information** to accompany Manuscript]

The thermal reorganization of DNA immobilized at the silica/buffer interface: a vibrational sum frequency generation investigation

*Zhiguo Li,** Champika N. Weeraman,** Md. Shafiul Azam, Eiman Osman and Julianne M. Gibbs-Davis**

Department of Chemistry, University of Alberta, Edmonton, Alberta T6G 2G2, Canada

Laser System and Experimental Setup. A detailed description of our SFG setup[1] and the design of the temperature-variable solid/liquid sample cell[2] have been described in previously published papers. Generally, the amplified 798-nm light pulses from the Spitfire were passed through a 30/70 beam splitter, and 2.3 W was used to pump a non-collinear optical parametric amplifier (TOPAS-C and NDFG, Light Conversion) to generate light in the IR, while some of the remaining 798-nm light passed through a Fabry-Perot etalon (TecOptics) to generate picosecond pulses (full width half maximum of 10 cm^{-1}). Each beam was focused at the sample using a CaF_2 (focal length = 500 mm, Thorlab) or BK7 (focal length = 400 mm, Thorlab) focusing lens, respectively. The IR polarization was horizontal to the table therefore perpendicular to the sample plane from the TOPAS NDFG (p-polarized), and the visible polarization was set to p or s using a half-wave plate (Thorlabs). Pulse energies of 10-20 μJ/pulse

of visible and ~10-20 μJ/pulse of IR were used, and the beams were slightly defocused to minimize sample damage. The infrared (fs) and visible (ps) pulses were directed through the IR grade silica hemisphere at incident angles of 66° and 64° with respect to surface normal. The sample cell was designed to place the flat surface of the hemisphere perpendicular to the laser table. This vertical arrangement allowed us to change the solvent at the interface without requiring a flow setup.

For all of the experiments, only one TOPAS-NDFG setting was used to collect the spectra centered near 2900 cm^{-1}. For data acquisition, 4W × 10H or 5W × 10H binning was used to reduce the noise and the data were acquired for 3-10 min per spectrum. The spectra shown in the figures are representative of at least two experiments. Although changes in the relative intensity of the peaks were observed from sample to sample, the peak position and the influence of hybridization state, strand composition, and temperature on the signal intensity was consistent and reproducible.

Sample Preparation. All oligonucleotides were synthesized on a solid-phase synthesizer (ABI 390) using reagents from Glen Research. All of the strands used contained a 5'-alkyne modified thymidine (Glen Research, Catalog No:10-1540-95) followed by the T_{15} or A_{15} sequence. This modified thymidine lacked a methyl group owing to the placement of the alkyne substituent. The benzyl azide monolayer for immobilizing the alkyne DNA was prepared following our previous publication with an increased reaction time of ~15 hours (overnight) between the *p*-trimethoxysilyl benzyl azide in toluene and the freshly cleaned silica surface to increase the monolayer density.[3] The DNA-functionalized samples were also prepared following our previous work[2] except that a 1:1 DMSO:ethanol rinse replaced pure DMSO. All buffers contained 0.5 M

NaCl, 10 mM PBS (pH 7) unless noted, and the final complementary strand concentration was 0.61 μM for duplex samples.

Determination of the Surface Density of Immobilized DNA Strand. The DNA surface was prepared by using our previously published strategy[2] with a longer deposition time of *p*-azidomethyl phenyltrimethoxysilane. X-ray photoelectron spectroscopy experiments indicated that the amount of surface nitrogen increased only slightly. Specifically, treating a Si wafer coated with a native oxide layer with the silane solution for 5 hours resulted in a N:O:Si ratio of 0.043:0.84:1. Increasing the reaction time for 15 hours resulted in a N:O:Si ratio of 0.052:0.81:1. The increase in the amount of nitrogen based on the increase in the N:Si or N:O ratio is indicative of a 20 or 25% increase, respectively, in azide compared with samples prepared in our previous publication.[2] For those samples a density of 6×10^{12} strand per cm^2 was estimated by assuming the silanol density was 3×10^{14} sites per cm^2 and that condensation with the p-azidobenzyl trimethoxy silane resulted in an azide density equal to 10% of the original silanol sites (this value represents an underestimation assuming far from complete condensation of all of the silanol sites). By using XPS, 15-30% of the azides were found to be converted to triazoles bearing DNA strands, which led to an approximate strand density of 6×10^{12} strands per cm^2. Although this density was calculated assuming the initial azide density, the resulting kinetic behavior was very consistent with a strand density of 10^{-7} mol per m^2 (~6×10^{12} strand per cm^2) based on the kinetic model of heterogeneous hybridization put forth by Krull and co-workers.[4] Based on the slight increase in azide content under the coupling conditions for this paper, a slightly higher strand density was expected, but according to the above model by Krull significant changes in the kinetic behavior is only expected when strand density varies by orders of magnitude.

SFG Spectra at the T_{15}-Functionalized Silica/D_2O Interface. Utilizing D_2O to avoid overlap between the O-H stretch of the strongly hydrogen bonded water and the stretch of the C-H groups led to poor spectra compared with that observed in water (Figures S1-3). To understand the strong solvent dependence of the spectra, we reason that enhanced overlap between the O-H stretch of water and the C-H stretches actually improved the signal of the latter due to constructive interference that led to signal enhancement (Figure S5). We attribute the weaker SF signal in the D_2O spectra to two factors: first, the polarizability of OD is expected to be weaker than that of OH[5] and this polarizability contributes to the hyperpolarizability and thus SFG activity.[6] Second, the overlap is less between the C-H stretches and the weakly hydrogen-bonded O-D stretch (around 2510 cm^{-1})[7] compared with the overlap between the C-H stretches and the strongly hydrogen-bonded O-H stretch (around 3200 cm^{-1}).[8] As the O-D peak is further from the C-H stretching region than the O-H peak, there is very weak resonance of D_2O in the C-H stretching region. Weak resonant enhancement of D_2O in this region is supported by the slightly higher SFG intensities at lower wavenumber for the D_2O spectrum in the absence of salt (Figures S1 and S2). As salt was added the amount of aligned D_2O diminished resulting in less resonant enhancement of the D_2O, similar to what was discussed and observed in Figure 1.

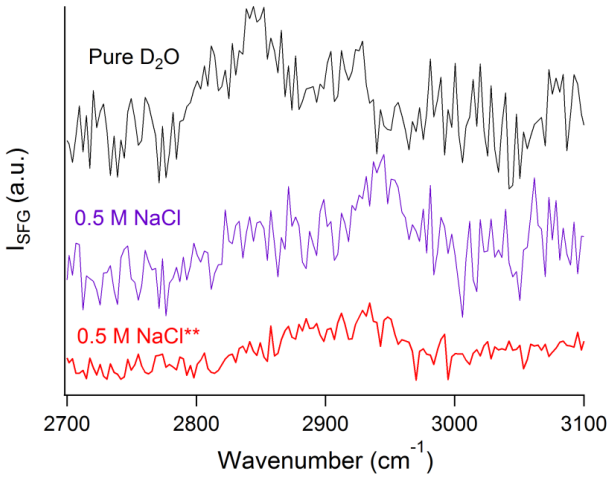

Figure S1. Raw (not normalized) ssp-SFG spectra at the T_{15}-functionalized silica/D_2O interface in pure D_2O and upon adding buffer (10 mM PBS, 0.5 M NaCl in D_2O, pH 7). **After hybridizing with the complementary strand.

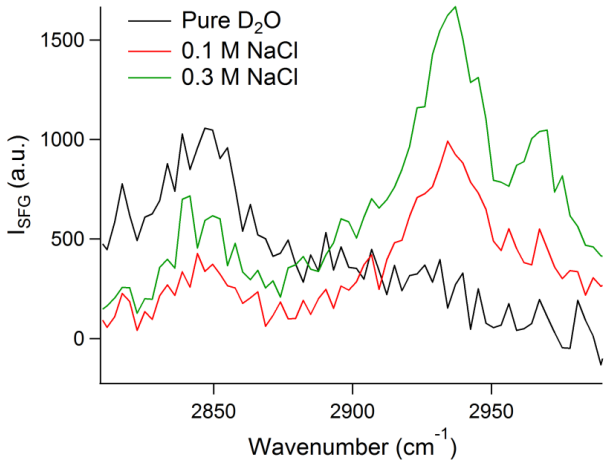

Figure S2. Raw ppp-SFG spectra of the same sample as shown above in Figure S1 at the T_{15}-functionalized silica/D_2O interface. The salt solutions were prepared using 10 mM PBS buffer (pH 7) in D_2O.

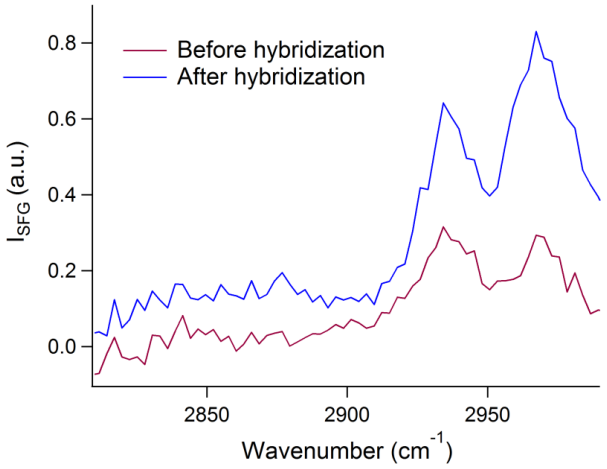

Figure S3. The gold normalized ppp-SFG spectra of the sample shown in Figure S1 before and after hybridization with A_{15} in solution. *Experimental conditions:* 0.61 μM A_{15}-T-alkyne in 0.5 M NaCl, 10 mM PBS at pH 7 in D_2O. The peak at ~2970 cm^{-1} is likely the asymmetric stretch of the methyl group of thymine.

SFG Spectra at Silica/H_2O and Silica/D_2O Interfaces. As shown in Figure S4, SFG spectra were collected from both silica/H_2O and silica/D_2O interfaces. In the C-H stretching region (2800-3000 cm^{-1}), both H_2O and D_2O have contribution to the SFG spectrum; however, the contribution from H_2O is more intense compared with that from D_2O (Figure S4A), which has been attributed to two factors as described before: the stronger polarizability of OH and the better overlap between the C-H stretches and strongly hydrogen-bonded O-H stretch. The normalized spectra in Figure S4B clearly shows the difference between the tail of strongly hydrogen-bonded O-H stretch, which has a center frequency of 3200 cm^{-1}, and the tail of weakly hydrogen-bonded O-D stretch, which has a center frequency of 2510 cm^{-1}.

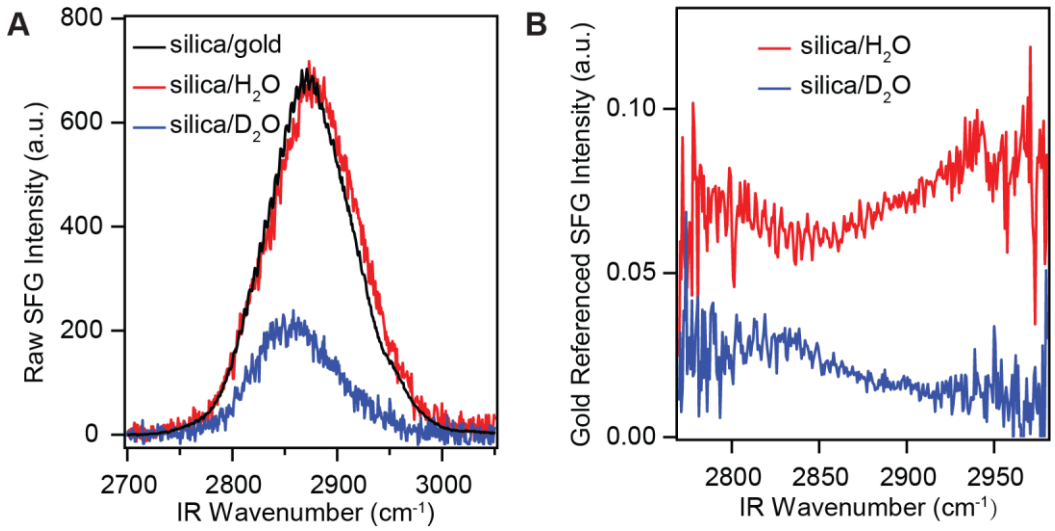

Figure S4. A) Raw SFG spectrum from silica/H_2O interface compared with that from the silica/D_2O interface at the same experimental configuration. The black trace represents spectrum collected from silica/gold interface, and its maximum intensity has been normalized to the same value as that of silica/H_2O spectrum. B) Gold normalized SFG spectra from silica/H_2O and silica/D_2O interface.

Interference between the C-H Stretch and O-H Stretch. In order to show how the interference between water's O-H stretch (3200 cm^{-1}, corresponding to strongly hydrogen bonded water) and the C-H stretches of DNA should affect the observed SFG spectra in the C-H stretch region, the following simple simulation has been done. In this example, the amplitude of the CH_3 symmetric stretch peak at 2877 cm^{-1} was set as a constant while the amplitude of the O-H peak at 3200 cm^{-1} was varied. For simplicity the nonresonant second order susceptibility was set to zero. For the C-H and O-H resonances, the following peak properties were assumed: for the CH_3 symmetric stretch, $\omega = 2877$ cm^{-1}, $\Gamma = 16$ cm^{-1}, $A = 1$; for the OH stretch, $\omega = 3200$ cm^{-1}, $\Gamma = 150$ cm^{-1}.

$$|\chi|^2 = |\chi_{CH} + \chi_{OH}|^2 = \left(\frac{1}{\omega - 2877 + 16i} + \frac{A}{\omega - 3200 + 150i}\right)\left(\frac{1}{\omega - 2877 - 16i} + \frac{A}{\omega - 3200 - 150i}\right)$$
$$= \frac{1}{(\omega - 2877)^2 + 256} + \frac{A^2}{(\omega - 3200)^2 + 22500} + \frac{2A\left[\omega^2 - 6077\omega + 9208800\right]}{\left[(\omega - 2877)^2 + 256\right]\left[(\omega - 3200)^2 + 22500\right]}$$
$$= \text{term}\,1 + \text{term}\,2 + \text{term}\,3$$

(Eq. S1)

In this equation, term 1 corresponds to the C-H stretching peak, term 2 corresponds to the O-H stretching peak, and term 3 is a cross term. Using a Gaussian expression for the IR intensity owing to the Gaussian shape of the IR pulse centered at 2900 cm^{-1} (bandwidth 120 cm^{-1}) and the three terms corresponding to $|\chi|^2$, SFG spectra were generated from:

$$I_{SFG} \propto |\chi|^2 I_{vis} I_{IR} \propto |\chi|^2 I_{IR} = |\chi|^2 \exp\left[-\frac{(\omega - 2900)^2}{14400}\right] \quad \text{(Eq. S2)}$$

Figure S5 shows the observed relative intensities of the three terms and overall observed SFG spectra at different O-H peak amplitudes. When the amplitude of the O-H peak is much greater than that of the C-H stretch peak, the observed overall SFG spectra is dominated by the O-H peak and the C-H peaks are difficult to distinguish. This explains the spectrum for the DNA-modified silica/Millipore interface observed at very low salt concentration, which corresponds to a large amount of ordered water molecules owing to the presence of many negative charges at the interface. As salt was added, the interfacial static electric field arising from the negatively charged DNA and silica was screened resulting in less ordered water and a lower amplitude for the O-H peak (as the amplitude is proportional to the number density of aligned water).[9] In contrast, adding salt did not severely impact the amplitude of the C-H resonances as the number density of DNA remained constant. Consequently, the C-H resonances became apparent with increasing salt concentration.

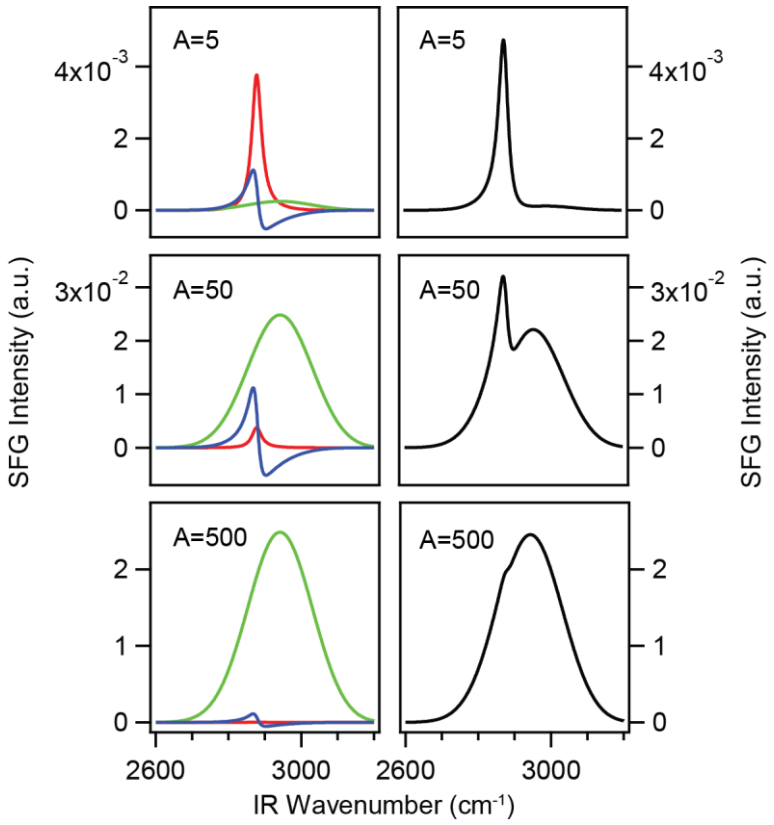

Figure S5. Simulated SFG spectra showing the interference between the water O-H stretch and a methyl C-H stretch. The spectra were modeled using equation S2. The amplitude of O-H peak (A) was varied and relative SFG intensities of the three terms were shown. The contribution to the signal of term 1 is shown in red, term 2 in green, and term 3 in blue. The overall observed spectra are in black on the right hand side.

Spectral Normalization. The spectra shown in Figures 2A, 3A, 4, S7, S9 and S11 were normalized as follows: After background subtraction, each spectrum from the DNA-silica/buffer aqueous salt interface was divided by the corresponding spectrum from the same sample at the pure water interface, as the signal was dominated by the water peak at low salt concentration. As shown in Figure S6, the spectrum of the DNA-modified silica/water interface has a similar Gaussian shape as that from the silica/gold interface, so we can use the DNA-modified surface/water interface to determine the shape of the IR pulse. This procedure has the advantage of not requiring sample replacement to collect the reference spectrum, which can introduce error due to imperfect realignment between the actual and reference samples.

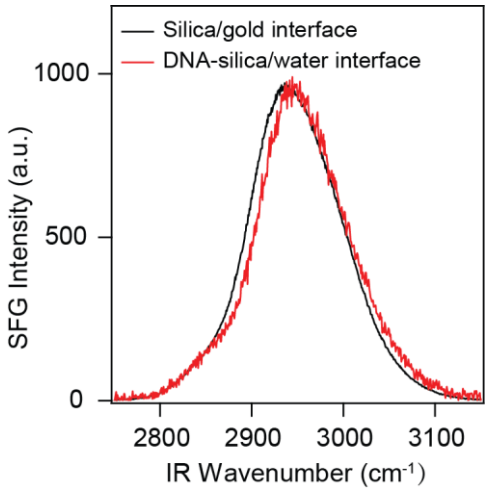

Figure S6. SFG spectrum from the DNA-silica/water interface compared with that from the silica/gold interface. The maximum intensities have been normalized to the same value as greater signal is always observed from the silica/gold interface owing to its greater second-order susceptibility compared with the silica/water interface.

The spectra shown in Figures 2B, S3 and S8 were normalized to the silica/gold interface, as gold exhibits strong non-resonant signal independent of IR wavelength. This referencing was achieved by dividing the spectra from DNA-functionalized sample with the spectrum measured immediately before from a gold-coated silica hemisphere at the same IR central wavelength (the same TOPAS-NDFG settings).

Spectral Fitting. The following equation was employed to fit the SFG spectra. The second order susceptibility $\chi^{(2)}$ is broken down into a non-resonant term $\chi_{NR}^{(2)}$, and vibrational resonant term $\chi_{R}^{(2)}$ summed over all possible wavenumbers. Each resonant mode is considered to possess a Lorentzian lineshape as shown below:

$$I_{SFG} \propto \left|\chi^{(2)}\right|^2 = \left|\chi_{NR}^{(2)} + \sum_v \chi_R^{(2)}\right|^2 = \left|\chi_{NR}^{(2)} + \sum_v \frac{A_v}{\omega_{IR} - \omega_v + i\Gamma_v}\right|^2 \quad \text{(Eq. S3)}$$

Here ω_{IR} is the wavenumber of the incident IR beam, and A_v, ω_v, and Γ_v are the amplitude, wavenumber, and damping coefficient of the v^{th} surface vibrational mode, respectively. The

fitting was accomplished using Igor Pro: based on the number of vibrational modes expected in the region, a function with the desired number of resonant terms and a non-resonant term was chosen for fitting. For each fitting, initial A_v, ω_v, Γ_v and $\chi^{(2)}_{NR}$ values were estimated around the central wavenumbers noted in the manuscript and then the software was allowed to optimize all of them; the returned values from the previous run were used as initial values for a second run. The fitting stopped when the returned values were the same as the previous input values. Then for the last run, all ω_v values were held as constants and the values of other parameters were obtained from fitting. The fitting parameters for Figure 2A and Figure 2B are shown in Table S1 and Table S2, respectively. The fitting parameters for Figure 3A and Figure S9 are shown in Table S3 and Table S4, and the corresponding peak amplitude/gamma ratios from each spectrum are plotted in Figure S12 and S13. The fitting parameters for Figure 4 and Figure S8 are shown in Table S5 and Table S6, respectively.

Comparison of Different Polarization Combinations. Figure S7 shows the ppp and ssp SFG spectra of the T_{15}:A_{15} modified surface at 20 °C. The strong peak at ~2975 cm^{-1} in the ppp spectrum is tentatively attributed to the CH_3 asymmetric stretch. Generally, we observed more contribution from the water in the ppp spectrum at the silica/water interface. This is supported by the slope of the background for the ppp spectrum shown below, which we attribute to residual water on the sample after DNA attachment.

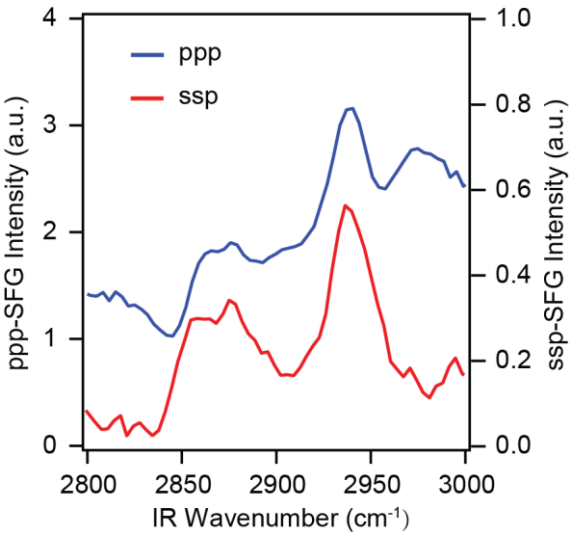

Figure S7. Different polarization combinations in the SFG experiment of the T_{15}:A_{15} modified surface collected at 20 °C.

SFG Spectra at the A_{15}-Functionalized Silica/Air Interface. As shown in Figure S8, SFG spectra were collected from A_{15}-functionalized silica/air interface under different polarizations. Four peaks were determined from fitting with central wavenumbers at 2862, 2881, 2923 and 2927 cm^{-1}, respectively, in ppp spectrum; at the same time, only one dominate peak at 2924 cm^{-1} was obtained in ssp spectrum. The detailed fitting parameters are shown in table S6.

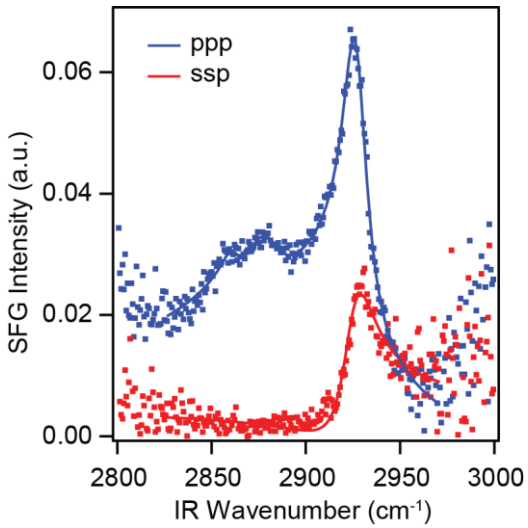

Figure S8. SFG spectrum collected at A_{15}-functionalized silica/air interface.

Thermal Evolution of Single-Stranded Immobilized DNA. Figure S9 shows the thermal evolution of the single-stranded oligonucleotide T_{15} immobilized at the silica/buffer interface. Overall the SFG signal gradually decreased from 20 to 60 °C, indicating thermal energy induced randomization of the strand conformation owing to increased conformation entropy at higher temperatures.

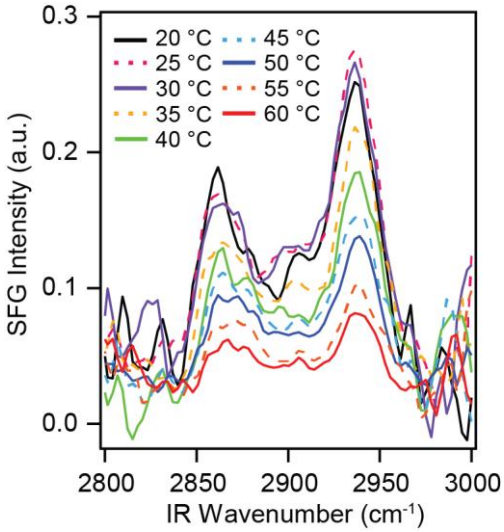

Figure S9. Changes in SFG intensity of the T_{15}-modified silica/buffer interface normalized to that of water as a function of temperature. The high signal-to-noise below 2845 cm^{-1} and above 2980 cm^{-1} is due to the lack of IR power at these wavenumbers and the normalization procedure.

Comparison of Thermal Dissociation Profiles of the Immobilized and Solution-Phase T_{15}:A_{15} Duplex. Our previous study utilizing second harmonic generation spectroscopy and the same copper-catalyzed azide-alkyne cycloaddition attachment strategy found that immobilization of a 15-mer onto silica suppressed the thermal dissociation, or melting, temperature (T_m) by approximately 12 ± 2 °C in comparison with its solution-phase melting temperature (Figure S10A).[2] To verify that the change in A/Γ (2937 cm^{-1}) SFG ratio versus temperature for the duplex system stemmed from duplex dissociation (Figure 3B and S10B), we compared it under the same conditions (0.61 μM primer, 0.5 M NaCl, 10 mM PBS buffer, pH 7.0) to the thermal dissociation of solution-phase DNA based on changes in UV absorbance at 260 nm (Figure S10B). To determine the melting temperature, the A/Γ ratio versus temperature in Figure S10B was fit with the following equation:

$$\text{Fraction Dissociated} = \frac{Ratio_{\max} - Ratio}{Ratio_{\max} - Ratio_{\min}} = \frac{1}{1+\exp\left(\frac{\Delta H}{R}\left(\frac{1}{T+273.15} - \frac{1}{T_m+273.15}\right)\right)} \quad \text{(Eq. S4)}$$

where ΔH is the dissociation enthalpy, T is the temperature of the solution phase in Celsius, T_m is the melting temperature in Celsius, R is the ideal gas constant, $Ratio_{max}$ and $Ratio_{min}$ are fitting parameters.[2] The absorbance at 260 nm (Abs) was converted to the fraction dissociated according to: Fraction dissociated=1-(Abs_{max}-Abs)/(Abs_{max}-Abs_{min}), which was also fit with equation S4. From the fit to the SFG and absorbance data, the T_m was determined to be 37.5 °C for the former (the immobilized duplex) and 49.4 °C for the latter (the solution-phase duplex). The difference between the solution-phase melting temperature and the melting temperature for the immobilized DNA duplex was therefore 11.9 °C, which is consistent with our previous study (12 ± 2 °C).

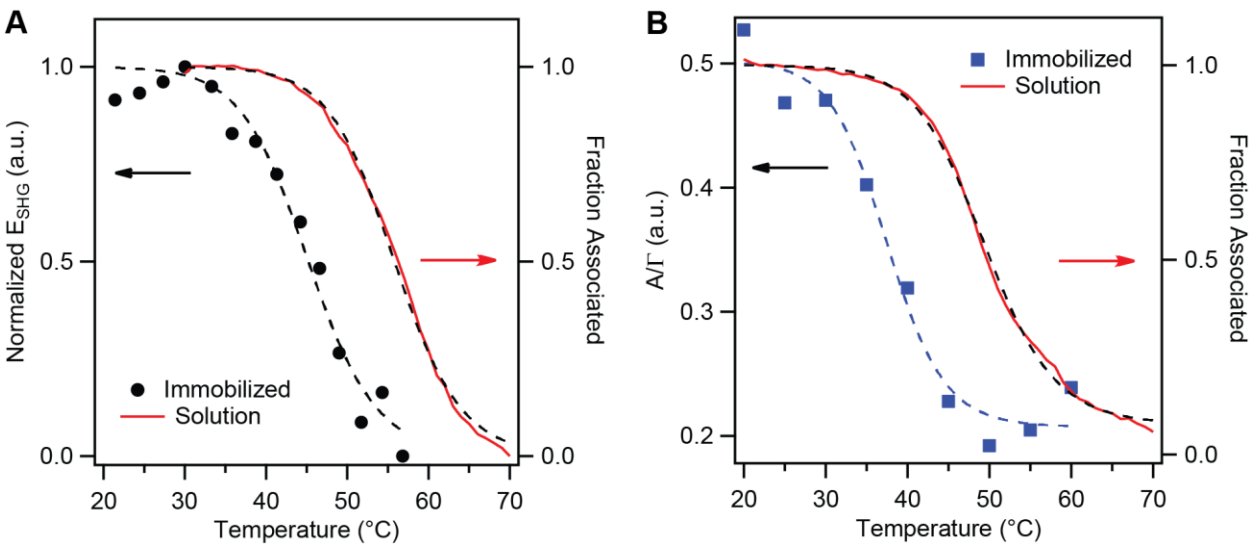

Figure S10. A) Thermal dissociation of a 15 base pair DNA duplex at the silica/water interface monitored by resonant SHG and the comparison with the corresponding melting curve in solution phase using the same immobilization chemistry. The melting temperature difference was determined to be approximately 12 ± 2 °C. The figure is re-created from reference 2. B) Comparison of the melting curve of the immobilized T_{15}:A_{15} duplex from the SFG A/Γ ratio (blue) and the free duplex in solution (red) based on absorbance measurements. *Reaction conditions:* 0.61 μM of each solution phase strand, 0.5 M NaCl, 10 mM PBS buffer, pH 7.0. The melting temperature difference was determined to be 11.9 °C very consistent with the results from the SHG study. The dashed lines are fits to the data with equation S4.

Thermal Dissociation Experiment in Solution. For DNA duplex melting experiment in solution, 0.61 nmol of each DNA sequence was mixed in 1.0 ml PBS buffer (0.5 M NaCl, 10 mM PBS, pH 7.0), and was allowed to equilibrate for 1 hour. The melting experiments were performed using Agilent 8453 UV-Visible Spectroscopy System with absorbance readings at 260 nm taken at 1 °C intervals from 20 to 70 °C. The hold time at each temperature was 1 min. The solution was stirred at 250 rpm during the temperature-variation experiment.

Annealing of the T_{15}-Functionalized Sample without Hybridization. SFG spectra have been collected from the T_{15}-functionalized silica/buffer interface before and after annealing the sample at 60 °C without hybridization to the A_{15} strand. Unlike the spectral changes for the T_{15}:A_{15} duplex (Figure 4), which were very consistent, the changes in spectra for the single strand varied from sample to sample (Figure S11).

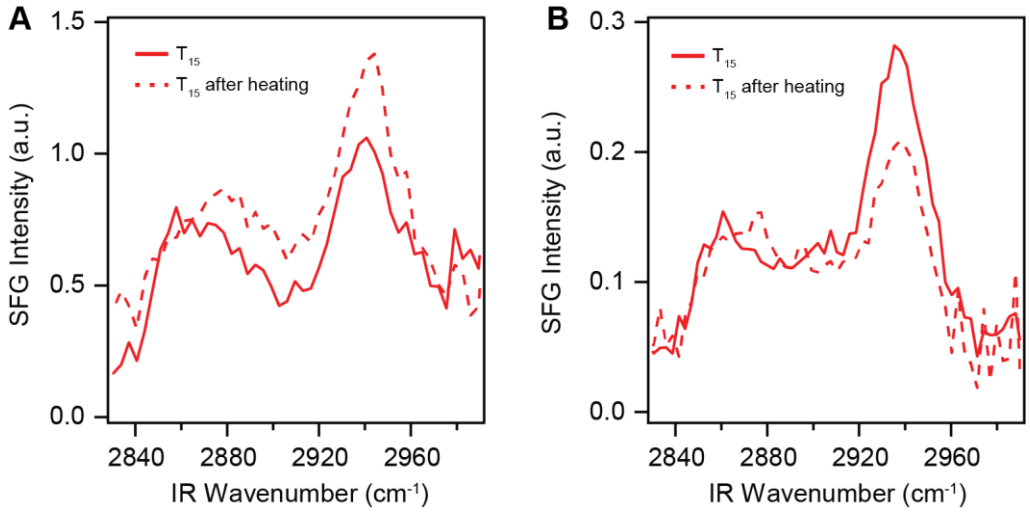

Figure S11. SFG spectra collected from the single-stranded T_{15}-functionalized silica/buffer interface before and after annealing the sample at 60 °C. The spectra were collected under the ssp polarization combination, and normalized to that from the DNA-functionalized silica/water interface. A) and B) represented spectra collected from two different samples under the same reaction conditions.

Table S1. Spectral Fitting Parameters for Figure 2A.

	ω	A^a	Γ	ω	A^a	Γ	ω	A^a	Γ	ω	A^a	Γ	ω	A^a	Γ
S[b]	**2856**	17.1(1.9)	26.7	**2878**	1.5(1.1)	8.7	**2895**	1.7(1.6)	13.7	**2924**	6.2(2.6)	17.4	**2936**	1.9(0.7)	9.5
D[b]	**2857**	7.8(2.8)	17.0	**2877**	9.9(1.2)	11.2	**2895**	5.8(2.8)	15.4	**2924**	2.3(2.3)	12.2	**2936**	9.7(2.1)	13.7

[a] The standard deviation of the amplitude returned from the fit is shown in parentheses.
[b] "S" represents single stand T_{15}, and "D" represents duplex T_{15}:A_{15}.

Table S2. Spectral Fitting Parameters for Figure 2B.

	ω	A^a	Γ	ω	A^a	Γ	ω	A^a	Γ	ω	A^a	Γ	ω	A^a	Γ
PPP	**2857**	2.8(0.2)	15.6	**2881**	1.9(0.1)	11.4	**2926**	4.9(0.4)	21.7	**2943**	0.6(0.2)	8.9	**2973**	0.9(0.1)	9.6
SSP	**2857**	1.1(0.2)	12.7	**2882**	1.3(0.1)	10.6	**2924**	1.2(0.4)	11.5	**2944**	2.6(0.5)	16.7	-	-	-

[a] The standard deviation of the amplitude returned from the fit is shown in parentheses.

Table S3. Spectral Fitting Parameters for Figure 3A.

T	ω	A^a	Γ	ω	A^a	Γ	ω	A^a	Γ	ω	A^a	Γ	ω	A^a	Γ
20	**2860**	2.2(0.6)	8.2	**2877**	5.9(1.0)	13.8	**2895**	2.3(1.0)	12.5	**2917**	2.6(1.0)	13.5	**2935**	6.2(0.8)	11.7
25	**2859**	1.7(0.5)	6.9	**2876**	6.3(1.3)	14.3	**2895**	2.7(1.6)	14.3	**2920**	2.8(1.4)	15.3	**2936**	5.1(0.9)	10.8
30	**2861**	1.7(0.5)	7.0	**2877**	5.4(1.1)	13.3	**2895**	2.4(1.3)	12.8	**2919**	3.0(1.5)	15.2	**2936**	5.3(1.0)	11.4
35	**2860**	1.8(0.6)	7.4	**2878**	5.9(1.2)	14.4	**2898**	2.1(1.6)	14.3	**2922**	3.4(1.6)	15.5	**2937**	3.9(0.9)	9.7
40	**2861**	1.8(0.7)	7.5	**2877**	6.4(1.6)	14.7	**2902**	2.6(2.2)	17.0	**2925**	3.4(1.4)	13.0	**2938**	2.5(0.7)	7.7
45	**2860**	1.7(0.8)	6.7	**2877**	6.1(2.3)	15.0	**2900**	3.6(3.3)	19.2	**2927**	3.1(1.6)	11.7	**2938**	1.7(0.6)	7.3
50	**2861**	1.6(0.7)	6.8	**2876**	5.9(1.9)	14.4	**2901**	3.5(2.7)	18.6	**2927**	3.4(1.5)	12.0	**2939**	1.2(0.6)	6.3
55	**2861**	1.6(0.7)	6.5	**2877**	6.6(1.9)	15.0	**2902**	3.2(2.6)	18.0	**2926**	2.9(1.4)	12.0	**2937**	1.4(0.5)	7.1
60	**2863**	1.7(0.6)	7.2	**2879**	5.8(1.3)	14.1	**2900**	3.7(1.9)	17.2	**2925**	3.0(1.2)	12.6	**2938**	1.8(0.5)	7.4

[a] The standard deviation of the amplitude returned from the fit is shown in parentheses.

Table S4. Spectral Fitting Parameters for Figure S9.

T	ω	A^a	Γ	ω	A^a	Γ	ω	A^a	Γ	ω	A^a	Γ	ω	A^a	Γ
20	**2864**	1.3(0.5)	6.6	**2880**	3.3(1.0)	14.4	**2906**	2.6(1.3)	13.0	**2927**	2.9(1.0)	12.5	**2939**	2.7(0.9)	10.1
25	**2861**	0.8(0.6)	6.5	**2873**	2.5(2.0)	12.2	**2902**	6.3(4.0)	22.8	**2926**	1.3(1.4)	11.5	**2936**	3.6(1.2)	11.3
30	**2861**	0.8(0.7)	6.7	**2873**	2.2(1.2)	10.2	**2900**	4.8(2.9)	19.2	**2924**	2.6(2.0)	15.1	**2935**	3.5(1.2)	11.8
35	**2862**	1.1(0.6)	8.1	**2876**	3.3(1.5)	14.7	**2902**	3.7(1.8)	16.8	**2924**	1.2(0.8)	11.4	**2936**	2.9(0.7)	10.4
40	**2864**	1.2(0.5)	6.3	**2878**	1.9(1.2)	10.3	**2898**	3.2(2.8)	17.3	**2924**	2.6(2.4)	15.6	**2936**	2.3(0.7)	10.4
45	**2865**	1.1(0.5)	7.6	**2880**	3.6(1.1)	15.7	**2904**	1.8(1.1)	12.9	**2924**	1.9(0.8)	12.9	**2937**	2.1(0.6)	10.5
50	**2862**	0.1(0.1)	2.0	**2874**	3.4(1.5)	16.6	**2901**	3.6(2.4)	22.1	**2927**	2.0(1.2)	14.8	**2939**	1.5(0.5)	9.4
55	**2861**	0.2(0.1)	3.3	**2874**	4.5(1.2)	18.7	**2907**	2.1(1.2)	16.4	**2924**	0.1(0.2)	4.0	**2935**	2.3(0.4)	11.3
60	**2865**	0.7(0.8)	9.0	**2879**	2.4(2.1)	16.1	**2905**	2.2(2.5)	16.3	**2926**	0.8(1.4)	13.5	**2937**	2.0(0.9)	11.8

[a] The standard deviation of the amplitude returned from the fit is shown in parentheses.

Table S5. Spectral Fitting Parameters for Figure 4.

	ω	A^a	Γ	ω	A^a	Γ	ω	A^a	Γ	ω	A^a	Γ	ω	A^a	Γ
I[b]	**2860**	2.2(0.6)	8.2	**2877**	5.9(1.0)	13.8	**2895**	2.3(1.0)	12.5	**2917**	2.6(1.0)	13.5	**2935**	6.2(0.8)	11.7
II[b]	**2859**	1.1(0.3)	6.9	**2879**	4.3(0.6)	11.5	**2894**	6.1(1.6)	19.2	**2928**	2.9(1.3)	14.9	**2938**	3.9(0.6)	10.3

[a] The standard deviation of the amplitude returned from the fit is shown in parentheses.
[b] "I" represents "before annealing", and "II" represents "after annealing".

Table S6. Spectral Fitting Parameters for Figure S8.

	ω	A^a	Γ	ω	A^a	Γ	ω	A^a	Γ	ω	A^a	Γ	ω	A^a	Γ
PPP	**2862**	0.10(0.06)	6.6	**2881**	0.5(0.2)	14.4	**2923**	5.4(0.7)	44.6	**2927**	1.0(0.1)	8.0	-	-	-
SSP	-	-	-	-	-	-	**2924**	1.24(0.05)	10.2	-	-	-	-	-	-

[a] The standard deviation of the amplitude returned from the fit is shown in parentheses.

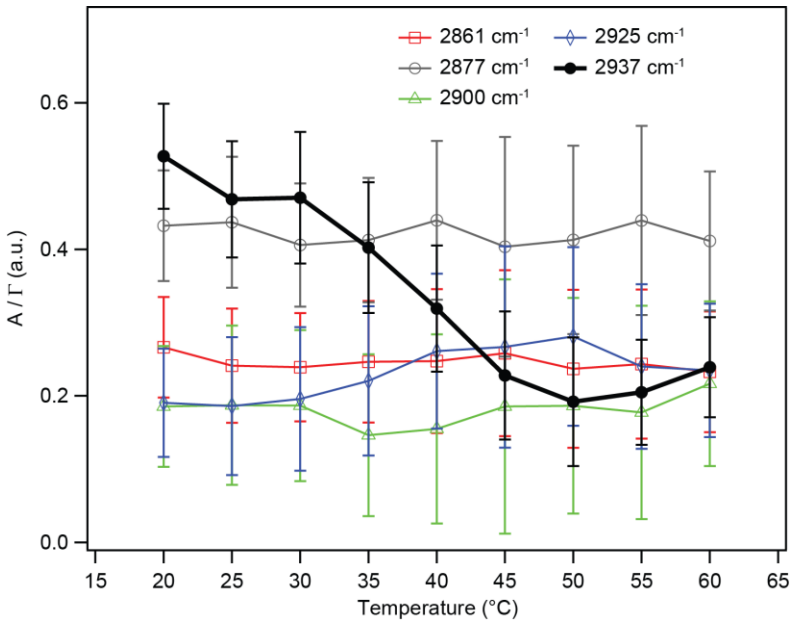

Figure S12. The ratio of peak amplitude to peak width (A/Γ) in Figure 3A as a function of temperature. The error bars are from the standard deviation of the amplitude returned from the fit.

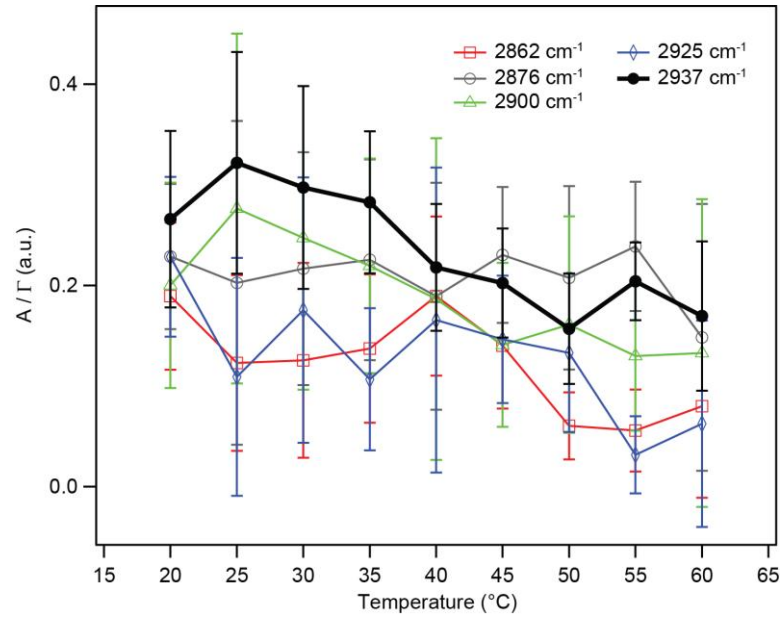

Figure S13. The ratio of peak amplitude to peak width (A/Γ) in Figure S9 as a function of temperature. The error bars are from the standard deviation of the amplitude returned from the fit.

Reference

1. M. S. Azam, C. N. Weeraman and J. M. Gibbs-Davis, *J. Phys. Chem. C*, 2013, 117, 8840-8850.
2. M. S. Azam and J. M. Gibbs-Davis, *Anal. Chem.*, 2013, 85, 8031-8038.
3. M. S. Azam, S. L. Fenwick and J. M. Gibbs-Davis, *Langmuir*, 2010, 27, 741-750.
4. D. Erickson, D. Li and U. J. Krull, *Anal. Biochem.*, 2003, 317, 186-200.
5. E. Tyrode and J. Hedberg, *J. Phys. Chem. C*, 2011, 116, 1080-1091.
6. R. D. Wampler, A. J. Moad, C. W. Moad, R. Heiland and G. J. Simpson, *Acc. Chem. Res.*, 2007, 40, 953-960.
7. P. B. Miranda, L. Xu, Y. R. Shen and M. Salmeron, *Phys. Rev. Lett.*, 1998, 81, 5876-5879.
8. Q. Du, E. Freysz and Y. R. Shen, *Phys. Rev. Lett.*, 1994, 72, 238-241.
9. K. C. Jena and D. K. Hore, *J. Phys. Chem. C*, 2009, 113, 15364-15372.